Ancient siderites reveal hot and humid super-greenhouse climate

Joep van Dijk[1], Alvaro Fernandez[1*], Stefano M. Bernasconi[1], Jeremy K. Caves Rugenstein[2,3] Simon R. Passey[4] and Tim White[5]

[1]Department of Earth Sciences, Geological Institute, ETH Zürich, Switzerland

[2]Max Planck Institute for Meteorology, Hamburg, Germany

[3]Seckenberg Biodiversity and Climate Research Center, Frankfurt, Germany

[4]CASP, West Building, Madingley Rise, Madingley Road, Cambridge CB3 0UD, UK

[5]Earth and Environmental Systems Institute, The Pennsylvania State University, PA, USA

*Now at Bjerknes Centre for Climate Research and Department of Earth Science, University of Bergen, Norway

Earth's climate is warming as the rise in atmospheric CO_2 (pCO_2) contributes to increased radiative forcing. State-of-the-art models calculate a wide range in Earth's climate sensitivities due to increasing pCO_2, and, in particular, the mechanisms responsible for amplification of high latitude temperatures remain highly debated. The geological record provides a means to evaluate the consequences of high radiative forcing on Earth's climate. Here we present clumped (Δ_{47}) and oxygen ($\delta^{18}O$) isotope data from latest Paleocene/earliest Eocene (LPEE; 57-55 million years ago) pedogenic siderites, a time when pCO_2 peaked between 1400 and 4000 ppm. Continental mean annual temperature reached 41 °C in the equatorial tropics, and summer temperatures reached 23 °C in the Arctic. Reconstruction of the oxygen isotopic composition of precipitation reveal that the hot LPEE climate was characterized by a globally averaged increase in specific humidity with a corresponding increase in the average residence time of atmospheric moisture and a decrease in the subtropical-to-polar specific humidity gradient compared to the present-day. Pedogenic siderite data from other ancient super-greenhouse periods support the evidence that with higher global mean

temperatures and a decreased meridional temperature gradient the increase in specific humidity is subject to polar amplification.

Continued anthropogenic emissions of CO_2 may increase Earth's radiative forcing to levels that were last encountered during the early Eocene Epoch (56-48 Ma ago)[1]. Thus, by investigating early Eocene paleoclimate records, we can evaluate the potential consequences of high radiative forcing on Earth's climate. The latest Paleocene/earliest Eocene is often studied as an analogue to ongoing climate change, as it involved a similar transient rise in pCO_2 (ref. [2]) and had a paleogeography similar to the present-day (Fig. S1). During the LPEE, Earth was effectively ice-free[3,4], with sea surface temperatures (SST) markedly warmer than present, with estimates ranging from 25 to 45 °C in the tropics[5] and from 10 to 23 °C in the polar latitudes[6,7] (Fig. 1B). Continental temperature records are even more uncertain, quantitative estimates of paleotropical temperatures are sparse (Fig. 1A), and there are only very few and uncertain temperature reconstructions from high latitudes[8,9]. Thus the limited number and spatial coverage of existing paleotemperature records inhibit their predictive power for the near-future[10]. Quantitative continental temperature reconstructions are needed to critically evaluate the SST record, and to progress understanding of temperature distributions in a super-greenhouse climate. Reconstructions can also provide constraints on how elevated pCO_2 results in larger temperature rises at high latitudes relative to the tropics, or polar amplification of temperature[11]. For example, the poleward migration of storm-tracks during the LPEE has been proposed to have delivered more precipitation and latent heat to the Arctic[12]. However, the source of the high-latitude precipitation is not clear, and state-of-the-art model simulations are not conclusive on the physical mechanisms responsible for this fundamental change in the hydrological cycle[13].

Here, we use the clumped isotope composition (Δ_{47}; see supplement) of pedogenic siderite spherules to construct a quantitative record of continental temperatures during the LPEE at sites that range from the equator to the Arctic. We expand this record with the first siderite-based meridional reconstruction of continental oxygen isotopes in precipitation during the LPEE ($\delta^{18}O_{precipitation}$; see supplement) to advance our understanding of the dynamics of the hydrological cycle under high radiative forcing. We collected siderites from thirteen paleosols that formed in freshwater wetlands (Fig. S17; Fig. 2), which developed in low elevation settings (<200 m.a.s.l.)[14] that became warmer and wetter during the LPEE. Locations, paleosols and siderites are described in detail in White *et al.* (2017) and in the supplement

(Fig. 2). All uncertainties in our reconstructions are reported at 2σ, or the 95% confidence level.

We find that Δ_{47}-based siderite temperatures decrease from 41 ± 6.2 °C in equatorial Colombia (3 °S), to 23-32 ± 8.2 °C in the temperate zones of North America and Europe (34 to 51 °N), to 35 ± 10.6 °C in southern Alaska (62 °N) and to 23 ± 7.9 °C in arctic Siberia (78 °N, Fig. 1). Depending on the latitude, pedogenic siderite formed at temperatures between the mean annual air temperature (MAT) and the mean air temperature of the warmest months (MWT) at the soil surface[15]. The exact temperature depends on the seasonal fluctuations in air temperature at the soil surface and the depth of siderite formation[15,16](Fig. S15). The temperature from Colombia represents MAT because during the LPEE the studied paleosol was located just below the equator where seasonal temperature fluctuations are low at any depth and because the vegetation cover in wetlands prevents any incident solar radiation from warming soil temperatures above air temperatures[15]. Our equatorial MAT reconstruction of 41 ± 6 °C may imply that most of the tropical C3-dominated forest biome, which persisted during the LPEE[17], would have conducted photosynthesis beyond their present-day photosynthetic optima[18].

Although our tropical temperature reconstruction likely represents MAT, siderites from temperate and high latitudes may show a bias toward the warmest months[15] because siderite precipitation is controlled by microbial iron reduction, which can proceed at faster rates when soil temperatures are higher[19]. However, none of our temperatures are entirely biased towards the MWT as all siderite spherules were retrieved from kaolinite-rich horizons that likely formed deeper than 100 cm in the subsurface during pedogenesis (see supplement), where seasonal temperature variability is damped[15]. Furthermore, seasonality in the continental interior of the US and arctic Siberia may have been reduced during the LPEE compared to the present-day[4,8,20,21], noting that some recent studies of super-greenhouse climates suggest seasonality in mid-continent settings was similar to the present-day[22–24]. Even if we assume present-day seasonality during the LPEE, our records in the temperate latitudes should be representative of MAT. For instance, the siderite from Alberhill, California (36 °N), formed at least one meter below the A-horizon, or lignite (Fig. S3), where modeling shows that most of the seasonal temperature variability – below 10 °C – is removed (Fig. S15). Nevertheless, the southern Alaskan and Siberian temperatures may still be slightly biased towards the MWT – despite a formation depth of 100 cm and possibly reduced LPEE seasonality – considering that present-day seasonal temperature variations exceed 10 °C at these latitudes. Thus, we consider that the temperatures presented here are representative of MAT from the tropics to temperate latitudes (0-51 °N/S), and they may have a measurable summer-bias – up to about 4 °C at a soil depth of 100 cm – at higher latitudes.

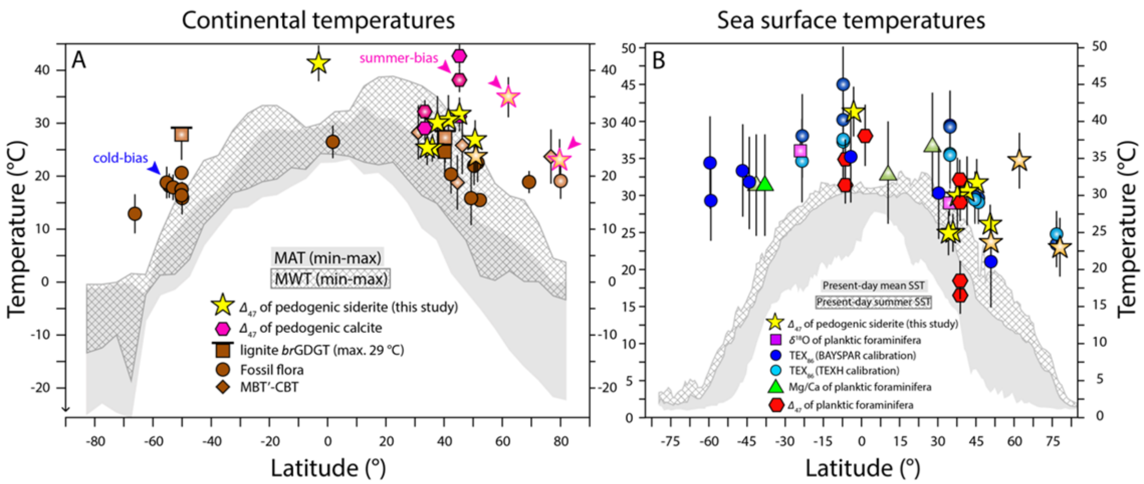

Figure 1: Temperature reconstructions during the latest Paleocene/ earliest Eocene. A) Compilation of LPEE continental temperature records at low elevation (below 200 m.a.s.l., with the exception of the pedogenic calcite data from the Bighorn Basin that represent a greater paleo-altitude) compared to the present-day maximum longitudinal temperature range for both MAT and MWT using the Worldclim 2 dataset at low elevation (see supplement and supplemental references). We use symbols with radial infill for PETM records, as the PETM represents the upper limit of LPEE warmth. Although some pedogenic calcite-based Δ_{47} temperatures are from >200 m.a.s.l., we included them to allow for a direct comparison to our siderite-based Δ_{47} temperatures at the same paleo-latitudes. Several records show a cold-bias in comparison to the siderite-based temperatures and the *br*GDGT-based temperatures in the temperate latitudes. Pink symbols are summer-biased (see text). Reconstructions are plotted with 1σ uncertainties at the LPEE paleo-latitudes (±2°). We refer to the supplement for a direct comparison of LPEE siderite temperatures and present-day temperatures (Fig. S12), and a compilation of LPEE temperatures from all elevations (Fig. S13). B) LPEE sea surface and siderite-based continental temperature reconstructions are directly compared to address the long-standing disagreement between both proxy records (see text). Sea surface temperature records represent 57-50 Ma and symbols with radial fills represent PETM records. All reconstructions are plotted with 1σ uncertainties. Both SST and continental records are best compared to the mean annual temperatures (grey) in the tropical and temperate latitudes, and to the warmest month temperatures (square pattern) in the high latitudes.

Our new continental temperature record shows that the LPEE was exceptionally hot with MAT being 6-24 °C warmer near the equator – significantly warmer than previously considered[9,25] – and MWT being 8-44 °C warmer in southern Alaska and 11-34 °C warmer in arctic Siberia, compared to the present-day range of mean annual and summer temperatures (Fig. S12). Our sample set consists of siderites formed during the latest Paleocene (57-56 Ma), Paleocene-Eocene Thermal Maximum (PETM, 56 Ma) and earliest Eocene (56-55 Ma, Fig. 1A), which may explain some variability in the temperature record. For instance, the extremely high temperature in southern Alaska records the PETM, which represents the upper limit of LPEE warmth. The PETM summer temperature in southern Alaska is 21 ± 11 °C warmer than the present-day summer temperature if we consider the present-day longitude and paleo-latitude (Fig. S12). In turn, our LPEE temperature reconstructions in the temperate zone (23 to 32 °C between 34 and 51 °N) are 0-25 °C warmer than the present-day temperatures (Fig. S12).

Our results support a cold-bias in some leaf physiognomic paleotemperatures[9] (Fig. S13) which could be related to the use of an empirical calibration that is not directly applicable to deep-time. We emphasize that the apparent cold-bias in leaf physiognomy in previous compilations[6] partially disappears when the paleo-elevation of the sites used for the reconstructions are considered (Fig. S13). Our record is in good agreement with the lignite *br*GDGT-based temperatures. As lignites probably represent a shallower soil depth than the siderite-bearing horizons (Fig. S15), the agreement between both records may suggest that seasonality in the temperate latitudes was reduced during the LPEE. Both temperature reconstructions could represent a lower limit on continental temperatures during the LPEE as they are from land surfaces that became wetter during the LPEE, which experience less warming than those that have become drier, as observed under the present-day rise in temperature[26,27]. Our siderite-based temperatures indicate that pedogenic calcite formation temperatures are summer-biased and perhaps affected by incident solar heating[28]. Last, our LPEE continental temperatures are very similar to LPEE SST reconstructions (Fig. 1B), resolving the long-standing disagreement between the two climate archives in the tropics and the mid-to-high Northern Hemisphere (NH) latitudes[9,29].

By combining the Δ_{47}-based temperatures with the δ^{18}O of the siderites we can reconstruct the δ^{18}O of the groundwater in which they formed. All siderites presented in this study formed in waterlogged soils in which the seasonal variations in the δ^{18}O of percolating rainwater would have been dampened (see supplement). Therefore, we consider that the reconstructed groundwater $\delta^{18}O$ records the mean $\delta^{18}O$ of precipitation ($\delta^{18}O_p$) at the site[15]. The $\delta^{18}O_p$ record (Fig. 2) confirms the robustness of our continental temperature record. The linear decrease in LPEE $\delta^{18}O_p$ from the equator to the high NH latitudes (Fig. 2) supports the notion that the siderites integrate a paleoclimatic signal that represents an averaged, maybe even regional temperature and $\delta^{18}O_p$ signal, and is not biased towards local conditions. Furthermore, the reduced poleward depletion in $\delta^{18}O_p$ confirms that the meridional temperature gradient was much reduced in the LPEE compared to the present-day.

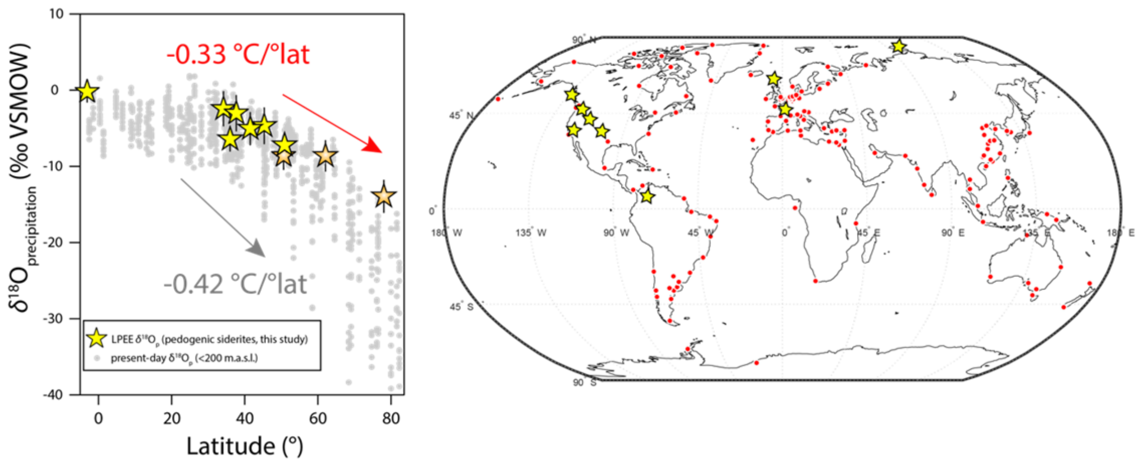

Figure 2: Siderite-based LPEE $\delta^{18}O_p$ reconstructions and modern GNIP $\delta^{18}O_p$ data (grey and red dots) for locations <200 m.a.s.l. from -3 to 80 °N and present-day and LPEE temperature gradients (see text). We use symbols with radial infill for PETM records, as the PETM represents the upper limit of LPEE warmth.

We can quantify the meridional temperature gradient using the decrease in $\delta^{18}O_p$ from the equator to the Arctic, which – unlike the high latitude siderite formation paleotemperatures – have no seasonal bias (see supplement). In the modern climate, $\delta^{18}O_p$ declines from the tropics toward the poles as air masses cool during transport poleward, reducing specific humidity, and preferentially removing ^{18}O from the atmospheric vapor reservoir. In the LPEE, the difference between the tropical $\delta^{18}O_p$ of 0.6 ± 0.4 ‰ and the polar $\delta^{18}O_p$ of -12.9 ± 1.6 ‰ is 13.5 ± 1.8 ‰. This translates into a difference in continental atmospheric paleotemperatures, between 3 °S and 78 °N – of 26 ± 3 °C, assuming a slope of 0.52 ‰ per °C for the relationship between $\delta^{18}O_p$ and atmospheric temperature[30]. We assume that this *global slope* is constant through time because both LGM[31] and early Eocene[32] isotope-enabled global circulation models (GCMs) predict little change in this relationship. This slope can be used to calculate ancient temperature gradients when the respective $\delta^{18}O_p$ reconstructions have a large latitude spread and are not biased by local or seasonal rainfall[33]. The reconstructed gradient of -26 ± 3 °C or -0.33 ± 0.03 °C/°lat agrees with the clumped isotope temperatures (Fig. 1A), supporting a summer-bias in the southern Alaskan and Arctic temperature reconstructions. It also agrees with the early Eocene sea surface temperature gradient of -21 ± 4 °C[34], again strengthening the agreement between our new continental climate reconstruction and existing ocean archives. Our reconstruction of the continental temperature gradient (-0.33 ± 0.03 °C/°lat) is greater than previously considered[6,29,35], and on the high side of the estimated sea surface temperature gradient[34]. However, it still confirms that the poles warmed significantly more than the tropics during the LPEE, considering that the present-day temperature gradient is -0.42 °C/°lat (Fig. 2).

Further, our $\delta^{18}O_p$ record improves our understanding of the atmospheric hydrological cycle during the LPEE. Globally elevated $\delta^{18}O_p$ (Fig. 3A) – corrected for the ice volume effect (see supplement) – indicates a decrease in the rainout of precipitable water, which leads to an increase in the residence time of moisture in the atmosphere[36] compared to the present-day. This change is driven by an increase in atmospheric specific humidity that is greater than the increase in global precipitation. Atmospheric vapor content increases at approximately the rate determined by the Clausius-Clapeyron relationship (~7.5%/K), whereas the increase in global mean precipitation is limited by energetic constraints to be substantially less (~2%/K)[37]. Because the atmospheric reservoir of water vapor is larger in a super-greenhouse climate, the removal of moisture from the atmosphere by precipitation will have a smaller effect on the $\delta^{18}O$ of precipitation than the same process today. This increase in specific humidity relative to precipitation results in an increase in the residence time of atmospheric moisture; today, $\delta^{18}O_p$ is positively correlated with moisture residence time[36,38], suggesting that the globally elevated LPEE $\delta^{18}O$ reflects this increase in residence time. Our geological evidence for globally elevated $\delta^{18}O_p$ in a super-greenhouse climate is new and supports a number of numerical modeling studies that find a dominant role for specific humidity and moisture residence time in determining the oxygen isotope composition of precipitation (refs. [38–43]).

There is, in addition, spatial structure in the $\delta^{18}O_p$ data that yields further insights into the atmospheric hydrological cycle in a super-greenhouse climate. In the modern climate, from approximately 10 ° to 40 °N/S evaporation is greater than precipitation (E > P), and this zone supplies moisture to both the tropics and the poles, where P > E. The datapoints outside this zone (equatorward of 10° and poleward of 40°) show the greatest enrichment in ^{18}O compared to today (Fig. 3A). Although we recognize that we only have one point in the tropics, we posit that this bimodal enrichment in ^{18}O at the equator and at the poles, with a relatively muted enrichment in the subtropics, results from latitudinal variations in net distillation in a super-greenhouse climate.

The observed increase in LPEE tropical $\delta^{18}O_p$ may seem counter-intuitive, as fully coupled and intermediate complexity models under high radiative forcing robustly predict a larger increase in precipitation over evaporation (*i.e.*, $\Delta P > \Delta E$) in the tropics[37,44]. Present-day tropical $\delta^{18}O_p$ values are frequently linked to the "amount effect", whereby greater precipitation results in a decrease in $\delta^{18}O_p$, as ^{18}O is removed faster than it can be re-supplied by evaporation or advection[43]. In the tropics the amount effect is expected to be greater during the LPEE due to a decrease in the frequency of precipitation events coupled to an increased intensity of each event[45]. Alternatively, we suggest that the observed higher LPEE tropical $\delta^{18}O_p$ is linked to an increase in specific humidity and average atmospheric moisture residence time. These increases result in reduced net moisture distillation and in an increase in $\delta^{18}O_p$ even with higher precipitation amounts. Such an effect has been observed in modern tropical precipitation during strong La Nina events[38]. Though speculative, we suggest that specific humidity increases overwhelm precipitation increases (and the associated amount effect) in the tropics because of the large increase in tropical temperatures ($\Delta T > 10°$) and also because of an increase in latent heat transport from the subtropics to the equator under high radiative forcing. The latter is postulated by intermediate complexity models for super-greenhouse climates[37,44]. Alternatively, the high $\Delta\delta^{18}O_p$ in equatorial Colombia could also reflect a regional decrease in P-E, despite a zonal-mean tropical increase in P-E, which would result in positive $\Delta\delta^{18}O_p$ due to a regional decrease in net distillation. Zonal variations in tropical P-E are large and changes in regional P-E may occur due to other processes such as changes in large-scale circulation and convection patterns[46]. More latitudinally resolved data are necessary to resolve these questions.

The increase in $\delta^{18}O_p$ in high latitudes – the largest in our dataset – is reflective of a global increase in specific humidity and reduced net poleward distillation of ^{18}O. Polar amplification of the warming results in a greater increase of specific humidity than of precipitation as it substantially reduces air mass cooling and net rainout during poleward moisture transport[12,32].

We suggest two possible mechanisms for this large increase in polar specific humidity: *(1)* An increase in latent heat transport from the subtropics, as postulated by some models (ref. [13,37]), or *(2)* high polar LPEE $\delta^{18}O_p$ could result from the initiation of local to regional deep convection under high radiative forcing[47] that also increases specific humidity more than precipitation. Though our dataset cannot distinguish between these mechanisms, in either case, the high, polar $\delta^{18}O_p$ results from greater global specific humidity and a reduced subtropical-to-pole gradient in specific humidity compared to the present-day.

Continental $\Delta\delta D_p$ reconstructions generally show more negative values (Fig. 3A) compared to our record of $\Delta\delta^{18}O_p$ (see supplement for a discussion). However, δD_p records associated with rising sea surface and continental temperatures within the LPEE may support the causality between high radiative forcing and high global specific humidity. Although changes in vegetation within the LPEE in both Colombia and Tanzania may have changed the effective hydrogen isotope fractionation in plants[17,48] and thus affected both δD_p reconstructions (Fig. 3A), the increase in tropical δD_p in Tanzania at 18 °S within the LPEE (ref. [48]) is consistent with increased specific humidity and atmospheric moisture residence time. The high LPEE $\Delta\delta D_p$ and increase in $\Delta\delta D_p$ within the LPEE in the Arctic at 80 °N (ref. [12]) are consistent with a decrease of the subtropical-to-pole specific humidity gradient.

We note that there are a number of further processes that may exert additional controls on $\delta^{18}O_p$ that may be both location- and climate state-dependent[41–43,49]. For example, state-shifts in stratocumulus clouds under high radiative forcing may alter cloud liquid droplet sizes thereby affecting $\delta^{18}O_p$ during hydrometeor descent[50,51]. Isotope-enabled climate simulations with improved cloud parameterizations[52] will prove instrumental to further evaluate the implications of our $\delta^{18}O_p$ reconstruction with regards to the hydrological cycle in a super-greenhouse climate. Nevertheless, the observed coherent changes in the latitudinal gradient of $\delta^{18}O_p$ (Fig. 2, 3A) suggests that planetary-scale changes, provide the first-order control on $\delta^{18}O_p$.

We cannot directly estimate specific humidity from our $\delta^{18}O_p$ data. However, we can use our siderite-based atmospheric temperature reconstructions to calculate saturation vapor pressures from equator-to-pole and use them as a proxy for specific humidity. To do so, we assume that specific humidity should increase according to Clausius-Clapeyron. We calculate the expected saturation vapor pressure using our temperature estimates and the August-Roche-Magnus equation[53] (Fig. 3B) and compare it to a calculation of saturation vapor pressure corresponding to an uniform warming of 15 °C from present-day temperatures (dashed line). This calculation shows the largest increase at the tropics and the smallest at the poles, following the exponential nature of the Clausius-Clapeyron relationship[37]. Our estimates of polar LPEE saturation vapor pressures are consistently greater than those expected from a uniform 15° warming, whereas the three subtropical datapoints are either equivalent to or lower. The greater increase at the poles shows that polar amplification of the warming results in a decrease of the specific humidity gradient between the subtropics and the poles. Quantifying the precise contribution of this decreased gradient either from enhanced poleward latent heat transfer, changes in moisture source regions and/or transport path[54] and local cloud feedbacks is not possible. However, we note that the robust, predicted increase in E-P in the subtropics and P–E at high latitudes[36,37,44] in models is suggestive of greater latent heat transport from the subtropics compared to the present-day[55].

The robustness of the observed LPEE patterns, can be evaluated by comparison with similar records from older super-greenhouse climates such as the late Permian/ early Triassic (~252 Mya) and Albian/ Cenomanian (~100 Mya) (Fig. S16) for which similar records are available. Although there is some variability in the data and the clumped isotope temperatures are missing, there is a striking similarity between tropical and polar oxygen isotope records from the three time periods. We propose that similar hot tropics and polar amplification may have existed in these time periods even though the paleogeography was very different from the present-day.

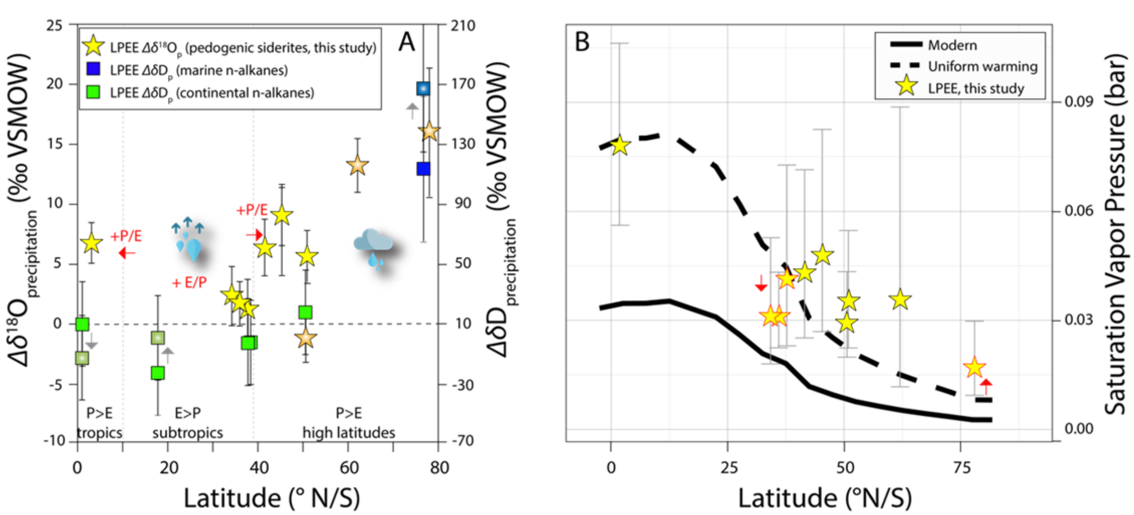

Figure 3: A) Siderite-based $\Delta\delta^{18}O_p$ and previous LPEE $\Delta\delta D_p$ reconstructions at low elevation (see text and supplement). Both records can be compared directly as the scales are designed to represent the meteoric water line ($\delta D_p = 8*\delta^{18}O_p + 10$). We use symbols with radial infill for PETM records, as the PETM represents the upper limit of LPEE warmth. We calculate $\Delta\delta^{18}O_p$ and $\Delta\delta D_p$ by subtracting the present-day $\delta^{18}O_p$ or δD_p at the site from the paleo-reconstruction after correction for the ice volume effect (see supplement). Globally, $\delta^{18}O_p$ is more positive during the LPEE due to a relatively larger increase in specific humidity compared to precipitation and the associated increase in the residence time of atmospheric moisture (see text). Tropical $\delta^{18}O_p$ may increase additionally due to an increase in the equatorward transport of water vapor (see text). High latitude $\delta^{18}O_p$ (and δD_p) may increase additionally due to a reduced subtropical-to-polar specific humidity gradient (see text). B) Saturation vapor pressure today (solid line), with a 15° uniform warming (dashed line), and estimated LPEE saturation vapor pressure using the siderite clumped temperatures in Figure 1 (stars). Error bars are min/max estimates using min/max estimates of LPEE temperature and temperature gradient. Red arrows and outlined star symbols depict the lower subtropical vapor pressures and higher polar vapor pressures relative to the uniform warming scenario.

The resolution and precision of the presented continental temperature and $\delta^{18}O_p$ dataset provide a unique opportunity to further improve climate simulations under high radiative forcing. It is encouraging that the latest global simulation of early Eocene climate that incorporate improved parameterizations of cloud microphysical processes and the shortwave cloud feedback[50] is in good agreement with our continental temperature reconstructions. Our datasets cannot resolve the relative contribution of different climate feedbacks (e.g. surface albedo, cloud, lapse rate, Planck, water vapor) and the role of meridional heat transport in realizing a high global average temperature and low meridional temperature gradient during the LPEE. Nevertheless, our data does provide the opportunity to test GCMs against a measure of climate that reflects the hydrological cycle: precipitation $\delta^{18}O$. The ability to simultaneously reproduce both super-greenhouse temperature and $\delta^{18}O_p$ records would further strengthen confidence in the models[52] and better constrain the mechanisms behind polar amplification in a warm, ice-free world.

It remains uncertain if the ongoing rapid increase in pCO_2 will give rise to a climate state similar to that of the LPEE[10]. Slow Earth system feedbacks (e.g. vegetation and ice cover) likely played a major role in maintaining warm conditions during the LPEE, and the strength of fast feedbacks (e.g. cloud condensation) may depend strongly on the background climate state (e.g. radiative forcing, vegetation and ice cover)[10]. Nevertheless, our coupled continental temperature and $\delta^{18}O_p$ reconstructions across the entire latitudinal range of the Northern Hemisphere provide a unique opportunity to evaluate changes in Earth's climate and atmospheric hydrological cycle under high pCO_2 conditions[10]. Our records show an exceptionally hot climate with hot tropics and subtropics that enabled humid and warm climates in the polar latitudes. This was probably true for the entire early Eocene and previous super-greenhouse climates with different geographical configurations. At the current rate of fossil-fuel combustion, the high radiative forcing that led to such a climate state multiple times in Earth's history, could be reached again in the foreseeable future[56].

Acknowledgements

We thank Madalina Jaggi and Stewart Bishop for assistance in the laboratory. We thank PAREX resources and G. Tellez for allowing sampling, and G. Bayona for identifying the siderite in the sample from Cuervos, Colombia. We thank G. Suan, J. Schnyder and F. Baudin for providing the sample from arctic Siberia. We thank M. Dechesne, E. D. Currano, R. Dunn and L. E. Schmidt for providing the sample from the Hanna Basin. We thank R. Peters for assistance with the Worldclim-2 and DEM data. We thank D. J. J. van Hinsbergen for assistance with the paleolatitudes. We thank C. Jaramillo, K. Snell, J. Kelson, E. Middlemas, D. Colwyn, T. Kukla, R. Wills and several anonymous reviewers for discussions. We acknowledge financial support through ETH project ETH-33 14-1 and Swiss SNF project 200021_169849.

Author contributions

TW and SMB designed the study. JD wrote the manuscript. JD, AFB and SMB developed the method for siderite analysis and JD and AFB performed the measurements. SRP provided the Faroese sample. TW provided most of the other samples. All authors contributed to discussions and editing of the final manuscript.

1. Foster, G. L., Royer, D. L. & Lunt, D. J. Future climate forcing potentially without precedent in the last 420 million years. *Nat. Commun.* **8**, 1–8 (2017).

2. Dickens, G. R., Castillo, M. M. & Walker, J. C. G. A blast of gas in the latest Paleocene : Simulating first-order effects of massive dissociation of oceanic methane hydrate. *Geology* 259–262 (1997).

3. Shackleton, N. J. & Kennett, J. P. Paleotemperature history of the Cenozoic and the

initiation of Antarctic glaciation; Oxygen and carbon isotope analyses in DSDP sites 277, 279 and 281. *Initial Reports Deep Sea Drill. Proj.* **29**, 743–755 (1975).

4. Wing, S. L. & Greenwood, D. R. Fossils and fossil climate: the case for equable continental interiors in the Eocene. *Philos. Trans. - R. Soc. London, B* **341**, 243–252 (1993).

5. Tierney, J. E., Sinninghe Damsté, J. S., Pancost, R. D., Sluijs, A. & Zachos, J. C. Eocene temperature gradients. *Nature Geoscience* vol. 10 538–539 (2017).

6. Hollis, C. J. *et al.* The DeepMIP contribution to PMIP4 : methodologies for selection , compilation and analysis of latest Paleocene and early Eocene climate proxy data , incorporating version 0 . 1 of the DeepMIP database. *Geosci. Model Dev. Discuss.* 1–98 (2019).

7. Evans, D. *et al.* Eocene greenhouse climate revealed by coupled clumped isotope-Mg/Ca thermometry. *Proc. Natl. Acad. Sci.* **115**, 1174–1179 (2018).

8. Suan, G. *et al.* Subtropical climate conditions and mangrove growth in Arctic Siberia during the early Eocene. *Geology* **45**, 539–542 (2017).

9. Naafs, B. D. A. *et al.* High temperatures in the terrestrial mid-latitudes during the early Palaeogene. *Nat. Geosci.* (2018) doi:10.1038/s41561-018-0199-0.

10. Caballero, R. & Huber, M. State-dependent climate sensitivity in past warm climates and its implications for future climate projections. *Proc. Natl. Acad. Sci. U. S. A.* **110**, 14162–7 (2013).

11. Pagani, M., Huber, M. & Sageman, B. *Greenhouse Climates*. *Treatise on Geochemistry: Second Edition* vol. 6 (Elsevier Ltd., 2013).

12. Pagani, M. *et al.* Arctic hydrology during global warming at the Palaeocene / Eocene thermal maximum. *Nature* (2006) doi:10.1038/nature05043.

13. Carmichael, M. J. *et al.* A model-model and data-model comparison for the early Eocene hydrological cycle. *Clim. Past* (2016) doi:10.5194/cp-12-455-2016.

14. White, T., Bradley, D., Haeussler, P. & Rowley, D. B. Late Paleocene–Early Eocene Paleosols and a New Measure of the Transport Distance of Alaska's Yakutat Terrane. *J. Geol.* **125**, 113–123 (2017).

15. van Dijk, J. *et al.* Experimental calibration of clumped isotopes in siderite between 8 . 5 and 62 ° C and its application as paleo-thermometer in paleosols. *Geochim. Cosmochim. Acta* **254**, 1–20 (2019).

16. Cermak, V., Bodri, L., Kresl, M., Dedecek, P. & Safanda, J. Eleven years of ground–air temperature tracking over different land cover types. *Int. J. Climatol.* **37**, 1084–1099 (2017).

17. Jaramillo, C. *et al.* Effects of rapid global warming at the paleocene-eocene boundary on neotropical vegetation. *Science (80-.).* (2010) doi:10.1126/science.1193833.

18. Berry, J. & Bjorkman, O. Photosynthetic Response and Adaptation to Temperature in Higher Plants. *Annu. Rev. Plant Physiol.* (1980) doi:10.1146/annurev.pp.31.060180.002423.

19. Silvola, J., Vaelijoki, J. & Aaltonen, H. Effect of draining and fertilization on soil respiration at three ameliorated peatland sites. . *Acta Forestia Fennica* vol. 191 1–32 (1985).

20. Eberle, J. J. *et al.* Seasonal variability in Arctic temperatures during early Eocene time. *Earth Planet. Sci. Lett.* **296**, 481–486 (2010).

21. Wolfe, A. P. *et al.* Pristine Early Eocene Wood Buried Deeply in Kimberlite from Northern Canada. *PLoS One* (2012) doi:10.1371/journal.pone.0045537.

22. Hyland, E. G., Huntington, K. W., Sheldon, N. D. & Reichgelt, T. Temperature seasonality in the North American continental interior during the Early Eocene Climatic Optimum. *Clim. Past* 1391–1404 (2018).

23. Snell, K. E. *et al.* Hot summers in the Bighorn Basin during the early Paleogene. *Geology* **41**, 55–58 (2013).

24. Burgener, L., Hyland, E., Huntington, K. W., Kelson, J. R. & Sewall, J. O. Revisiting the equable climate problem during the Late Cretaceous greenhouse using paleosol carbonate clumped isotope temperatures from the Campanian of the Western Interior Basin, USA. *Palaeogeogr. Palaeoclimatol. Palaeoecol.* (2019) doi:10.1016/j.palaeo.2018.12.004.

25. Shukla, A., Mehrotra, R. C., Spicer, R. A., Spicer, T. E. V. & Kumar, M. Cool equatorial terrestrial temperatures and the South Asian monsoon in the Early Eocene:

Evidence from the Gurha Mine, Rajasthan, India. *Palaeogeogr. Palaeoclimatol. Palaeoecol.* (2014) doi:10.1016/j.palaeo.2014.08.004.

26. Byrne, M. P. & O'Gorman, P. A. Trends in continental temperature and humidity directly linked to ocean warming. *Proc. Natl. Acad. Sci. U. S. A.* (2018) doi:10.1073/pnas.1722312115.

27. Seneviratne, S. I., Lüthi, D., Litschi, M. & Schär, C. Land-atmosphere coupling and climate change in Europe. *Nature* (2006) doi:10.1038/nature05095.

28. Quade, J., Eiler, J., Daëron, M. & Achyuthan, H. The clumped isotope geothermometer in soil and paleosol carbonate. *Geochim. Cosmochim. Acta* **105**, 92–107 (2013).

29. Huber, M. & Caballero, R. The early Eocene equable climate problem revisited. *Clim. Past* **7**, 603–633 (2011).

30. Yurtsever, Y. Worldwide survey of stable isotopes in precipitation. *Rep. Sect. Isot. Hydrol., IAEA* 40 (1975).

31. Lee, J. E., Fung, I., DePaolo, D. J. & Otto-Bliesner, B. Water isotopes during the Last Glacial Maximum: New general circulation model calculations. *J. Geophys. Res. Atmos.* (2008) doi:10.1029/2008JD0098597.

32. Speelman, E. N. *et al.* Modeling the influence of a reduced equator-to-pole sea surface temperature gradient on the distribution of water isotopes in the Early/Middle Eocene. *Earth Planet. Sci. Lett.* **298**, 57–65 (2010).

33. Fricke, H. C. & O'Neil, J. R. The correlation between 18O/16O ratios of meteoric water and surface temperature: Its use in investigating terrestrial climate change over geologic time. *Earth Planet. Sci. Lett.* **170**, 181–196 (1999).

34. Cramwinckel, M. J. *et al.* Synchronous tropical and polar temperature evolution in the Eocene. *Nature* **559**, 382–386 (2018).

35. Barron, E. J. Eocene equator-to-pole surface ocean temperatures: A significant climate problem? *Paleoceanography* **2**, 729–739 (1987).

36. Singh, H. K. A., Bitz, C. M., Donohoe, A., Nusbaumer, J. & Noone, D. C. A mathematical framework for analysis of water tracers. Part II: Understanding large-scale perturbations in the hydrological cycle due to CO2 doubling. *J. Clim.* (2016)

doi:10.1175/JCLI-D-16-0293.1.

37. Held, I. & Soden, B. Robust responses of the hydrological cycle to global warming. *J. Clim.* **19**, 5686–5699 (2006).

38. Aggarwal, P. K. *et al.* Stable isotopes in global precipitation: A unified interpretation based on atmospheric moisture residence time. *Geophys. Res. Lett.* (2012) doi:10.1029/2012GL051937.

39. Winnick, M. J., Caves, J. K. & Chamberlain, C. P. A Mechanistic Analysis of Early Eocene Latitudinal Gradients of Isotopes in Precipitation. *Geophys. Res. Lett.* **42**, 8216–8224 (2015).

40. Kukla, T., Winnick, M. J., Maher, K., Ibarra, D. E. & Chamberlain, C. P. The Sensitivity of Terrestrial δ 18 O Gradients to Hydroclimate Evolution. *J. Geophys. Res. Atmos.* (2019) doi:10.1029/2018JD029571.

41. Noone, D. & Simmonds, I. Associations between δ18O of water and climate parameters in a simulation of atmospheric circulation for 1979-95. *J. Clim.* (2002) doi:10.1175/1520-0442(2002)015<3150:ABOOWA>2.0.CO;2.

42. Rozanski, K. Isotopes in atmospheric moisture. in *Isotopes in the Water Cycle: Past, Present and Future of a Developing Science* (2005). doi:10.1007/1-4020-3023-1_18.

43. Moore, M., Kuang, Z. & Blossey, P. N. A moisture budget perspective of the amount effect. *Geophys. Res. Lett.* (2014) doi:10.1002/2013GL058302.

44. Siler, N., Roe, G. H. & Armour, K. C. Insights into the zonal-mean response of the hydrologic cycle to global warming from a diffusive energy balance model. *J. Clim.* JCLI-D-18-0081.1 (2018) doi:10.1175/JCLI-D-18-0081.1.

45. Carmichael, M. J., Pancost, R. D. & Lunt, D. J. Changes in the occurrence of extreme precipitation events at the Paleocene–Eocene thermal maximum. *Earth Planet. Sci. Lett.* (2018) doi:10.1016/j.epsl.2018.08.005.

46. Wills, R. C., Byrne, M. P. & Schneider, T. Thermodynamic and dynamic controls on changes in the zonally anomalous hydrological cycle. *Geophys. Res. Lett.* (2016) doi:10.1002/2016GL068418.

47. Abbot, D. S. & Tziperman, E. Sea ice, high-latitude convection, and equable climates.

Geophys. Res. Lett. (2008) doi:10.1029/2007GL032286.

48. Handley, L., Pearson, P. N., McMillan, I. K. & Pancost, R. D. Large terrestrial and marine carbon and hydrogen isotope excursions in a new Paleocene/Eocene boundary section from Tanzania. *Earth Planet. Sci. Lett.* **275**, 17–25 (2008).

49. Aggarwal, P. K. *et al.* Proportions of convective and stratiform precipitation revealed in water isotope ratios. *Nat. Geosci.* (2016) doi:10.1038/ngeo2739.

50. Zhu, J., Poulsen, C. J. & Tierney, J. E. Simulation of Eocene extreme warmth and high climate sensitivity through cloud feedbacks. *Sci. Adv.* (2019) doi:10.1126/sciadv.aax1874.

51. Schneider, T., Kaul, C. M. & Pressel, K. G. Possible climate transitions from breakup of stratocumulus decks under greenhouse warming. *Nat. Geosci.* (2019) doi:10.1038/s41561-019-0310-1.

52. Zhu, J. *et al.* Simulation of early Eocene water isotopes using an Earth system model and its implication for past climate reconstruction. *Earth Planet. Sci. Lett.* (2020) doi:10.1016/j.epsl.2020.116164.

53. Alduchov, O. A. & Eskridge, R. E. Improved Magnus form approximation of saturation vapor pressure. *J. Appl. Meteorol.* (1996) doi:10.1175/1520-0450(1996)035<0601:IMFAOS>2.0.CO;2.

54. Kavanaugh, J. L. & Cuffey, K. M. Space and time variation of δ18O and δD in Antarctic precipitation revisited. *Global Biogeochem. Cycles* **17**, (2003).

55. Donohoe, A., Armour, K. C., Roe, G. H., Battisti, D. S. & Hahn, L. The Partitioning of Meridional Heat Transport from the Last Glacial Maximum to CO 2 Quadrupling in Coupled Climate Models . *J. Clim.* (2020) doi:10.1175/jcli-d-19-0797.1.

56. IPCC. *Fifth Assessment Report (AR5)*. *Climate Change 2014: Synthesis Report. Contribution of Working Groups I, II and III to the Fifth Assessment Report of the Intergovernmental Panel on Climate Change* (2014) doi:10.1017/CBO9781107415324.